ARTICLES

Fingered morphology of niobium (110) grown by molecular-beam epitaxy

G. L. Zhou and C. P. Flynn
Materials Research Laboratory, University of Illinois at Urbana, Urbana, Illinois 61801
(Received 8 June 1998)

We report a regime of temperature film thickness and substrate miscut in which thin films of niobium (110) grow faceted on sapphire $(11\bar{2}0)$, and with a surface morphology that contains long fingers oriented along the niobium in-plane [001] direction. The origins of these features are discussed. [S0163-1829(99)06011-7]

I. INTRODUCTION

This paper concerns buffer layers of refractory metals grown epitaxially on sapphire. In recent years these have been developed as a valuable route to the synthesis of new epitaxial systems for use in scientific and technical applications. The first metals, grown with high quality by molecular beam epitaxy (MBE), were bcc Nb and Ta (Ref. 1) in several orientations that correspond to different cuts of the sapphire substrates and provide various alternative templates for chosen epilayers; still earlier research employed sputtering.[2] fcc iridium and hcp ruthenium[3] were also grown by MBE as epitaxial crystals of high quality, and other bcc metals such as Cr (Ref. 4) have since been synthesized. These various materials have been employed as templates to grow hcp rare earths in (0001) (Ref. 5) and $(1\bar{1}00)$ (Ref. 6) and $(1\bar{1}02)$ (Ref. 7) orientations and with tuned tilt,[8] intermetallic compounds like $L1_2Cu_3Au$ (Ref. 9) and the cubic Laves phase $TbFe_2$,[10] and remain for the future as a likely pathway for the synthesis of a wide variety of new epitaxial crystals. As such, the buffers themselves warrant careful study aimed at understanding and improvement of the template growth. The present paper reports new morphologies for Nb (110) films grown by MBE using methods that are now well established.

The manifest uses of these epitaxial crystals have attracted much interest and a variety of investigations have been reported. These mainly employ x rays for examination of Nb (110) crystal quality[11–14] and studies of Al_2O_3 surface evolution when annealed, and the consequences for Nb epitaxy,[15] and electron microscopy for exploration of the Nb-Al_2O_3 interface both for Nb (110) (Ref. 16) and other orientations.[17] Much less attention has been given to the morphology of the Nb epilayer itself, and the present paper is focused largely on this specific topic. The deficiency of information has no doubt arisen because the subject matter falls between the interests of surface scientists who typically use atomic force microscopy and scanning tunneling microscopy, but on the surfaces of bulk crystals, and the interests of solid state and materials scientists who are interested in heteroepitaxy but typically employ Fourier transform probes such as x-ray diffraction. Interest in the area is stimulated by a recent demonstration[18] that Nb grown by MBE under standard conditions can create striking surface mesostructures. In addition, these mesostructures of a refractory buffer material can be employed as templates for the synthesis of selected structural characteristics during subsequent epilayer growth. An example is the suppression of symmetry-allowed variants by mesostructures associated with vicinal miscut,[18] and the consequent elimination of incoherent twin boundaries from the resulting materials. There is a clear need for a better understanding of morphology in the growth of the refractory buffers.

In what follows we describe the dependence of morphology on structure in films of Nb (110) grown on commercially available substrates cut and polished on the sapphire *a* plane, specifically Al_2O_3 $(11\bar{2}0)$. It turns out that the kinetic processes involved in the evolution are complex, depending on several variables including vicinal miscut, growth rate, growth temperature, and film thickness, so that a complete analysis would be extremely time consuming. A great deal of work will be required to acquire a comprehensive understanding of film morphology for the range of interesting buffer materials, and in the several pertinent orientations. In the research reported here a small start is made on this agenda for the example of Nb (110) alone. Section II gives brief comments about crystal growth. The experimental studies of film structure are then described in Sec. III and discussed in Sec. IV. Section V provides a brief summary of the work.

II. CRYSTAL GROWTH

The epitaxial crystals grown on this work were synthesized by MBE on epitaxially polished Al_2O_3 $(11\bar{2}0)$ obtained from Johnson Matthey Co. During growth these were clamped by Ta wires to the Ta baseplate of the substrate heater. A Nb growth rate of 0.1–0.2 ML/s was employed throughout, in an MBE chamber that is described elsewhere.[1] It provided a base pressure in the mid 10^{-10} torr range. The actual pressure of residual gas, mostly H from the Nb charge, was about 3×10^{-9} torr during growth with the Nb *e*-beam hearth operational. While these are not particularly clean conditions, owing to the age of the system, it is our belief that residual gases play little or no part in the morphological evolution reported here.

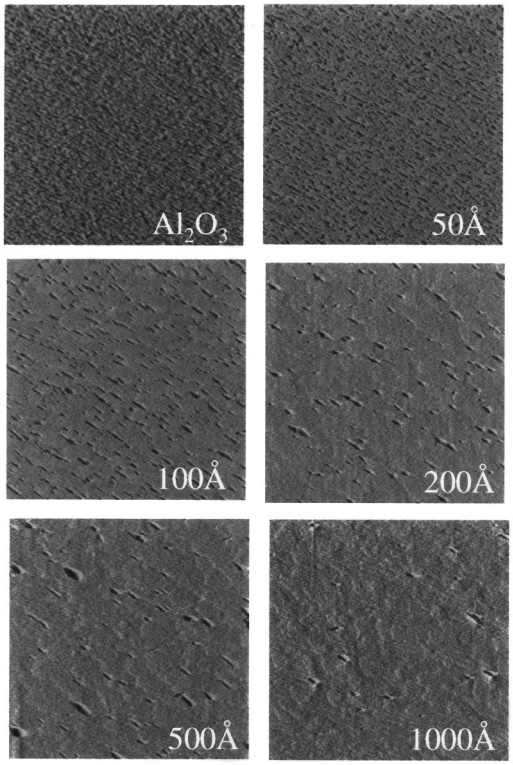

FIG. 1. AFM images of Nb (110) films of different thicknesses grown on low-miscut sapphire $(11\bar{2}0)$ (top left) at 900 °C. The films are fairly smooth, with pinholes that fill in thick films. The images are 2.1 μm across.

III. RESULTS

In this section we present results of experiment in which Nb (110) films grown on Al_2O_3 $(11\bar{2}0)$ are examined using atomic force microscopy, electron microscopy, and x-ray diffraction. The AFM results are reported first in order to characterize the Nb mesostructures that are the main result of this research.

A. Surface images by atomic force microscopy

Specimens were removed from the growth chamber and examined by force microscopy usually within a few days. It is our belief that no major changes in surface morphology occurred between growth and the AFM measurements, although a thin layer of surface contamination is undoubtedly present. A TopoMetrix system in the University of Illinois Beckman Institute was employed in the contact mode to acquire the data. These results reveal a morphology that depends systematically on the growth temperature and film thickness, and also on the vicinal miscut of the sapphire substrate. In Fig. 1 are shown AFM scans of a 2 μm$\times$2 μm area for five thicknesses of Nb grown on sapphire $(11\bar{2}0)$ with almost no miscut. The surfaces exhibit only weak features, other than pinholes that are mostly filled in the 1000-Å-thick film. The surface structure is greatly changed when the substrates have a 0.72°, miscut at 50° to Nb [001], yielding the Nb surfaces imaged in Fig. 2. Figure 2(a) gives results for 1000-Å-thick films grown at temperatures between 700 °C and 1000 °C, while part (b) of Fig. 2 shows how the

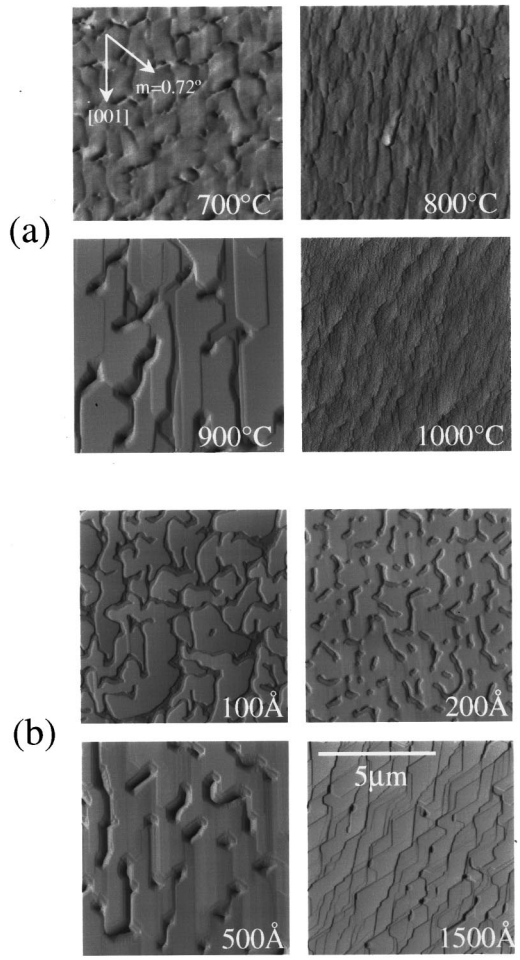

FIG. 2. (a) Nb (110) films 1000 Å thick grown at different temperatures on sapphire $(11\bar{2}0)$ with the miscut shown; and (b) films with different thicknesses grown at 1000 °C. All images are 2.1 μm across except the lower right in (b). Note the [001] fingers that occur at intermediate temperatures and thicknesses.

structure changes with film thickness for a growth temperature of 1000 °C. These sets of images reveal surfaces that are rough for low growth temperatures and thin films ~100 A thick, and that become smooth at high growth temperatures of 900–1000 °C and for films ~1000 Å thick. Films less than 200 A thick are formed from islands that are in the early stage of coalescence, while the surfaces of thick films grown at 1000 °C are either smooth or have wide faceted steps. Of special interest here are intermediate conditions under which the films in Fig. 2 can be seen to develop long fingers oriented along [001], with faceted tips that are identified more precisely below.

A variety of fingered structures in films 500–1000 A thick grown between 900 °C and 1000 °C for several miscuts are presented in Fig. 3. Two of these clearly reveal the ⟨111⟩ in-plane orientation of the fingertips. We infer that the dominant process in the fingering regime is faceting on the Nb {011} planes, which entirely define the finger surfaces. This is illustrated in Fig. 4 by line scans across AFM images for two films grown at 900 °C with 0.66° miscut and, respectively, 100 Å and 500 Å thick. In each case the Nb surface has faceted into a (110) plane tilted by the miscut with respect to the average sapphire surface. The fingers terminate

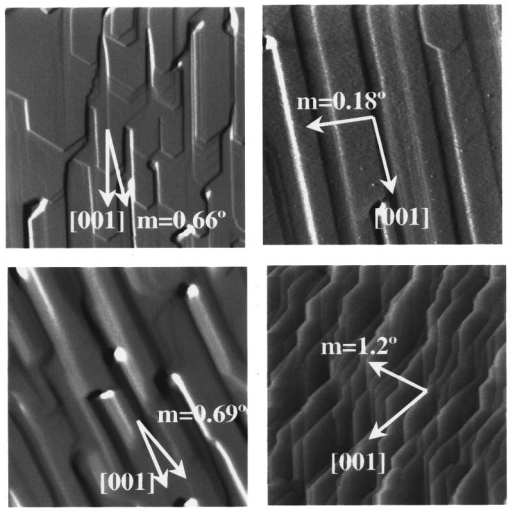

FIG. 3. Faceted Nb (110) surfaces grown at 900–1000 °C on sapphire $(11\bar{2}0)$ with various miscuts for films 500–1000 Å thick. All images are 2.1 μm across.

abruptly with ~20 nm discontinuities to leave a well-developed sawtooth structure in the thicker sample, with deep overshoots marking pinholes. In the most strongly fingered samples we presume that the fingertips are (011) and (101) planes, which each lie at 45° to the (110) surface plane, and that the edges of the fingers along [001] are $(1\bar{1}0)$ planes that lie perpendicular to the (110) surface. In this regime the pinholes appear faceted also, with the same planes apparently prevalent.

A further feature of the fingered structure is that the persistent pinholes are frequently located near the termini of the fingers. This is clarified in the images collected in Fig. 5 for a 500-Å film grown at 900 °C on a substrate miscut by 0.72° in the direction indicated. There, deep pinholes contrast with the smooth (110) surface. The image also shows that the surface contains numerous (110) ledges, and that these ledges pass into further faceted structures that are contained in the walls of the pinholes, for example at location *A* in the image, and in the inset enlargement. Other elaborate structures of a similar type, also with {110} facets, are apparent at *B* and *C*.

The results collected here establish that the fingered morphology is created by faceting in an intermediate regime of

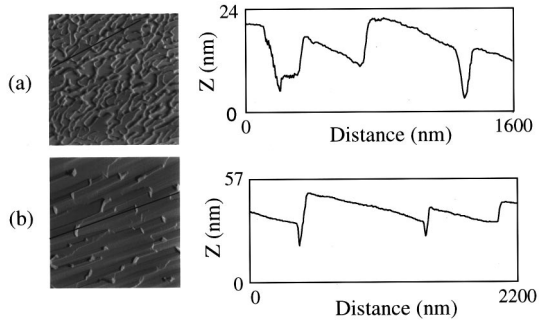

FIG. 4. AFM images and the line scans marked by straight lines for two Nb (110) films grown 100 and 500 Å thick at 900 °C on sapphire $(11\bar{2}0)$ miscut by 0.66°. The surface facets to (110) with step bunches ~20 nm high near pinholes.

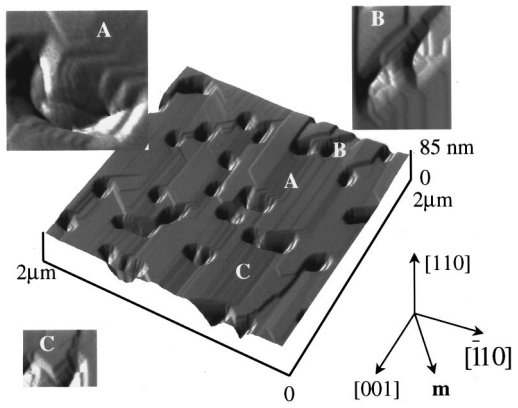

FIG. 5. AFM images of Nb (110) grown 500 Å thick at 900 °C on sapphire $(11\bar{2}0)$ miscut by 0.72° as indicated. Inset are shown details of surface ledge structures and elaborate structures on the pinhole walls, at the pinholes marked by letters.

temperatures and film thicknesses that depends also on the magnitude and direction of the sapphire miscut. This is the structure on which the present paper is focused.

B. Analysis using transmission microscopy

Plan view transmission electron microscopy (TEM) provides a powerful tool for the study of defect structures in epitaxial crystals.[19] Specimens were prepared by conventional methods[20] in the present research. A chosen area was first thinned from the back to about 30 μm by means of a dimpler, and then sputtered by an Ar^+ ion beam inclined at an angle of about 12°–15° to the plane of the sample. TEM observations were then carried out in a Philips EM420 electron microscope operating with a 120 keV beam.

Figure 6 contains bright field micrographs of a 500-Å-thick Nb (110) crystal grown at 900 °C on Al_2O_3 $(11\bar{2}0)$ miscut by 0.7°. The images are filled with moiré fringes that

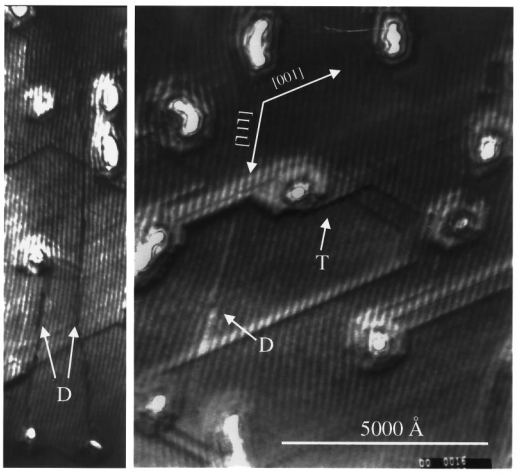

FIG. 6. Plan view TEM images of Nb (110) grown 500 Å thick at 900 °C on sapphire $(11\bar{2}0)$. The images are filled with moiré fringes from interference between the Nb and sapphire periodicities. (a) Bent Moire fringes indicate strains in the Nb that occur markedly near the faceted pinholes. *D* marks a dislocation and *T* the bent fringes near a fingertip. (b) Black lines are dislocations that thread from one pinhole to another.

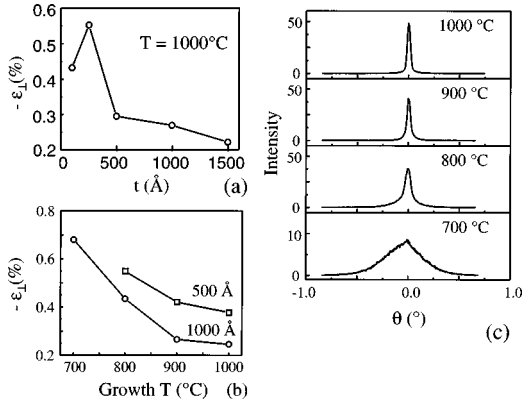

FIG. 7. (a) and (b) show the strain along the growth direction in Nb (110) films grown on sapphire $(11\bar{2}0)$ as functions of growth temperature and thickness. The data are obtained by measuring the centers of x-ray Bragg scans. The progressive strain relief with temperature and thickness is consistent with strain-layer theory. (c) shows how the rocking curve develops a broad component as the growth temperature is lowered.

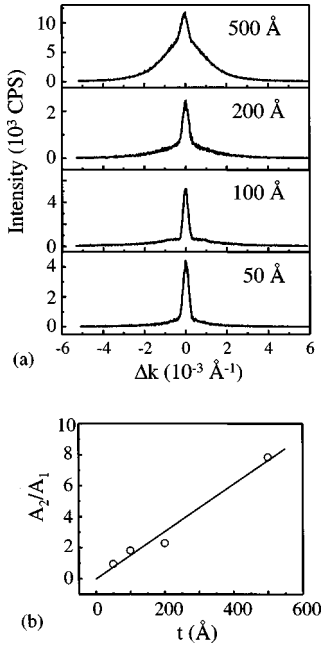

FIG. 8. Proportions of broad and narrow components in the x-ray rocking curves of Nb (110) films grown at 900 °C on sapphire $(11\bar{2}0)$ change with film thickness. (a) shows the transverse scans and (b) the ratio of the broad to narrow area.

arise when similar periodicities in the Nb and sapphire beat against each other.[21] Various structural features are clearly visible in the main panel of Fig. 6 (right). These include finger structures with edges along [001] as seen also by AFM, dislocations (see, e.g., *D*) in the moiré pattern that identify real dislocations in the Nb lattice, and also pinholes spaced on a length scale of one-half micron. The pinholes are markedly faceted along the [001] and ⟨111⟩ directions in agreement with the AFM results. It is clear from the image that the pinholes impede and terminate the fingers. In the left panel of Fig. 6 the long dark lines are dislocations that originate and terminate at pinholes.

It is an important point that the moiré fringes are sensitive to lattice strain, since any strain in the Nb lattice must alter the beat pattern. Note, then, that the fringes are strongly deformed near the pinholes, which establishes that the pinholes are associated with strong lattice deformations. These are large enough to leave dislocations when the pinholes are filled in. A circuit of the pinhole to the lower right in Fig. 6, for example, reveals two fewer moiré fringes beneath the pinhole than above. Each shift by one fringe indicates one missing plane of the corresponding lattice. Therefore, two edge dislocations must be left in the lattice as this particular pinhole is annealed away. It is readily verified by inspection that similar misfits occur near other pinholes. In contrast, there is little sign of added inhomogeneous strain at the [001] edges of the fingers, which thus cause no significant perturbation on the underlying material.

C. X-ray diffraction results

A D-max Rigaku powder diffractometer with 2 kW source was used with Cu $K\alpha$ radiation to examine a variety of films by x-ray diffraction. The available collimation offered a best resolution of about 0.05°.

Previous investigations have established that the diffraction peaks exhibit interesting structure.[13,14] Figure 7 collects some results of x-ray scans on Nb (110) films from the present work. In longitudinal (Bragg) scans the resolved α_1-α_2 splitting shows that the linewidth is limited by the instrument resolution and the sample thickness, with little added broadening from imperfections (see below). Figure 7(a) shows how the average strain along the growth direction in the Nb lattice at room temperature, obtained from the line center in Bragg scans, decreases systematically with thickness for Nb films more than 200 Å thick grown at 1000 °C. This strain relaxation with increased thickness is expected from strain-layer theory.[22] Further systematic behavior is visible in Fig. 7(b) which shows how the observed strain, as obtained from the Bragg peak center, varies as a function of the growth temperature, for two series of Nb (110) films, respectively, 500 and 1000 Å thick. As expected, the higher growth temperatures promote strain relief and permit a greater relaxation of the material towards its bulk lattice parameter. In Fig. 7(c), rocking (transverse) scans for films of various thicknesses are seen to comprise two components, one broad and one narrow, the latter resolution limited, much as reported in earlier research.[13,14] It is apparent for the thickest film that the centers of the two components are offset. The narrow component is found only on diffraction peaks that are located in reciprocal space perpendicular to the sample surface and is absent for off-axis peaks such as $(1\bar{2}1)$. The narrow and broad rocking components exhibit similar longitudinal scans.

In Fig. 8(a) are shown rocking scans for four Nb (110) films grown at 900 °C with different thicknesses on a substrate miscut by 0.7° along Nb [001]; part (b) shows how the relative areas of the narrow and broad components of these results vary systematically with film thickness. While the two components have comparable areas at 50 Å, the narrow portion is reduced to 10–15 % at 500 Å. In seeking the origin of the broad component of the Nb (110) reflection, Fig. 9 presents (110) and (220) rocking scans taken on a 500-Å film. From the fact that the broad component has approxi-

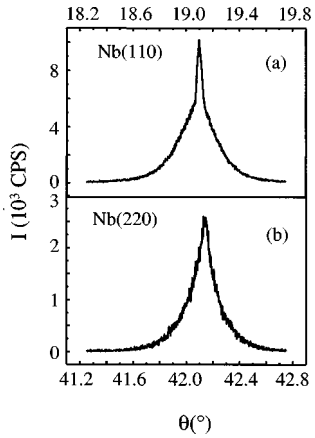

FIG. 9. The angular widths of the Nb rocking curves remain similar for (110) and (220) scans, which identifies the broad component as a mosaic spread.

mately the same angular spread in the two cases, we infer that this width arises mainly from a mosaic spread caused by tilted (110) lattice planes in the samples.

It has not been observed in earlier research that the broad component of the rocking curve is strongly anisotropic. This is revealed by the contour plot in Fig. 10(a) for a 500-Å film with 0.7° miscut oriented close to [001]. Part (b) of the figure shows the fingered surface morphology for this same sample.

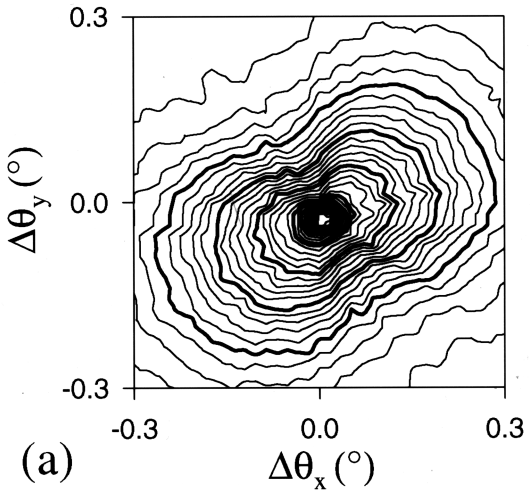

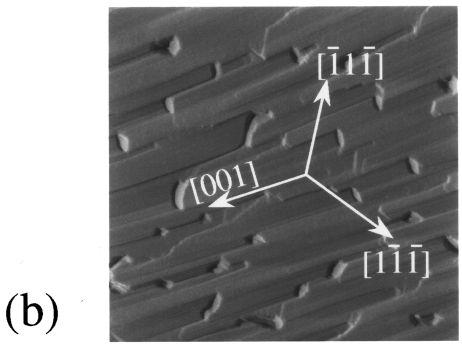

FIG. 10. (a) Anisotropy of the rocking curve for the fingered specimen shown with the same orientation in (b). The sample was miscut by 0.7° along [0001].

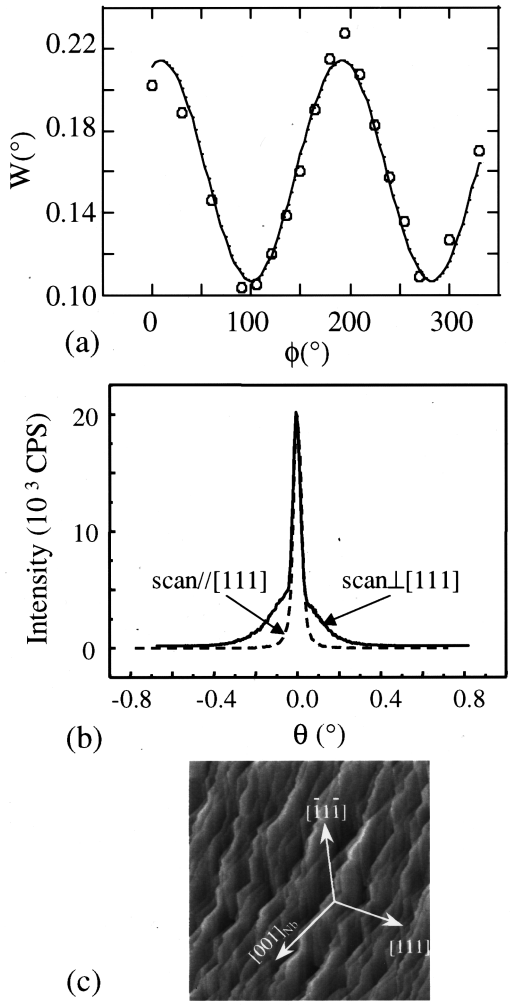

FIG. 11. (a) Anisotropy of the rocking curve width shown in (b) for the faceted sample whose AFM image is given in (c). The miscut was 1.2° along Nb $[\bar{1}1\bar{1}]$.

The greatest width of the rocking curve is closely aligned with the fingers and hence with the miscut for this sample. The fact that the greatest width lies approximately along [001] then points to the presence of lattice planes which exhibit their strongest buckling along this azimuth. In a second case, illustrated in Fig. 11, the surface is faceted but not fingered owing to a relatively large miscut of 1.2° along Nb $[\bar{1}11]$ in a film 1000-Å thick. Part (a) shows the x-ray profile both parallel and perpendicular to $[\bar{1}1\bar{1}]$. The scan along $[\bar{1}1\bar{1}]$ again has a broad component, which is lacking from the perpendicular scan. The variation of width with orientation is shown in (b) and the surface morphology in (c). These cases leave unresolved the relationship between the broad component and morphology, and this is clarified by the third example, shown in Fig. 12. Here the substrate is miscut along Nb $[1\bar{1}1]$, and the 1000-Å film was grown at high temperature and consequently lacks strong surface structure [Fig. 12(b)]. The Bragg scan in Fig. 10(a) shows the Nb (110) peak with α_1 and α_2 components visible and with interference oscillations that arise from the parallel top and bottom surfaces of the Nb. The point of interest here is that the scan along the $[1\bar{1}\,1]$ direction once more shows little or

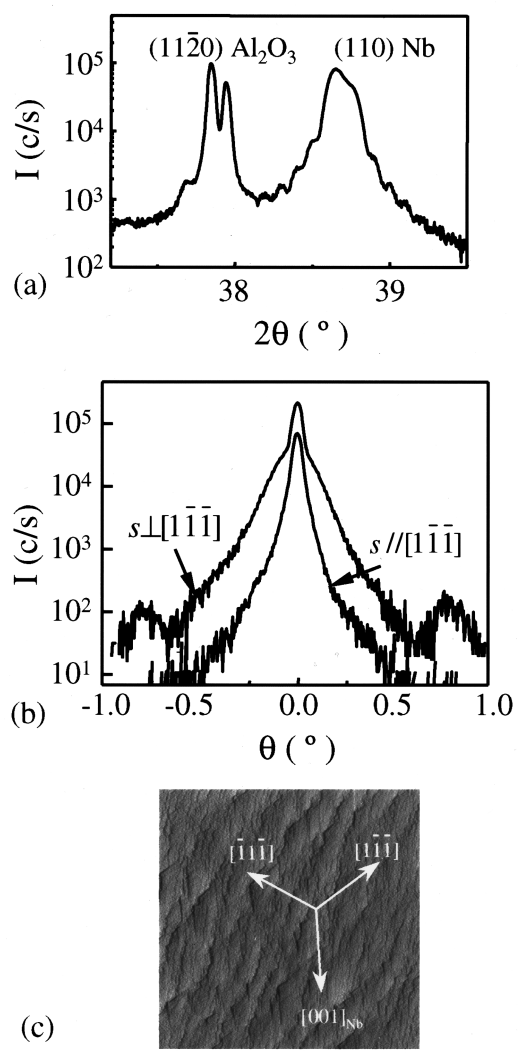

FIG. 12. (a) Bragg scan for 1000-Å-thick Nb (110) film grown on sapphire (11$\bar{2}$0) with 0.72° miscut along Nb [1$\bar{1}$1]. The α_1-α_2 splitting of the peak is visible, together with interference oscillations from the parallel front and back surfaces. The widest and narrowest rocking curves are shown in (b) and the smooth surface morphology in (c). Sidebands visible at ±0.7° on the wide curve in (b) are discussed in the text.

no broad component, which is, however, present perpendicular to [1$\bar{1}$ 1] and thus closer to the miscut direction.

From these and similar results we conclude that the broad component has no direct connection with morphology. Instead it is a general characteristic of Nb (110) films for this regime of conditions. The direction of least broadening is oriented close to the particular Nb ⟨111⟩ direction, which lies approximately perpendicular to the miscut direction.

A further feature in Fig. 12 warrants comment. The rocking curve along the miscut direction displays clear if weak sidebands, displaced from the central peak by approximately the magnitude of the miscut (0.72°). Sidebands of this type were first reported by Gibaud *et al.*,[14] who associate them with surface structure originating from the miscut.

IV. DISCUSSION

In the results reported above, thin films and low growth temperatures clearly lead to rough, highly strained films, while at high temperatures and for thick films the epitaxial strain is more relaxed and the film surfaces have mostly smoothed. Neither of these characteristics is remarkable because the more strongly activated mixing at high temperatures and the accumulation of bulk strain for thicker films lead to smoothing of the surface and to dislocation processes that relieve the epitaxial strain. What remains of great interest is the fingered morphology that emerges under intermediate conditions in samples with a variety of substantial miscuts. The discussion that follows is focused mainly on these interesting observations.

A coarse interpretation of the results identifies faceting, pinholes, and lattice strain as the primary ingredients in the energy balances that lead to the observed evolution of the fingered structures. Since material from the molecular beam falls everywhere almost equally, it follows from the observed persistence of deep pinholes that Nb atoms deposited in these areas must migrate elsewhere with greater probability than in the reverse process. Any net flow in a system at uniform temperature indicates that the chemical potential is greater at the source than at the sink. We can regard nonstatistical fluctuations of height as a record of this type of flow. It is then natural in the present example to attribute the fluxes from the pinholes to the fingers to the strong lattice strains in the neighborhood of the pinholes, which are identified unambiguously by the electron microscope images. The excess free energy associated with atoms in the strained region must drive the flow and cause the persistence of pinholes with the growth of fingers. Correspondingly, the decay of the pinholes in thick films at high temperature may be attributed to stress relief, no doubt by dislocation processes, which relaxes the lattice near the pinholes and thus eliminates the forces that bias the atomic fluxes. The fingers and the pinholes eventually disappear together.

Forces that can drive fingered growth are readily recognized in the geometry of the faceting process itself. Faceting is the result of steps that flow across the surface planes and bunch at the edges. For the bcc (110) surface the preferred steps lie along the ⟨111⟩ near-neighbor directions, and the flow occurs perpendicular to these steps. For the observed [001] fingers the steps flow diagonally across the finger and terminate on the perpendicular sides and on the fingertips, which lie at 45° to the surface plane. Atoms can accrete by diffusion fluxes on the top surface of the fingers only by diffusing up the perpendicular (1$\bar{1}$0) edge facets or up the 45° fingertip facets. Height differences in the surface profiles must therefore be attributed to these processes alone. The latter route requires that the atoms pass two 45° edges while in the former paths the edges have 90° angles. It seems certain that the 90° edges present the greater kinetic barrier and therefore that an enhanced portion of the inhomogeneous flow passes up the 45° facets at the fingertips. This bias can only be exaggerated further by the fact that the tips tend to neighbor pinholes, and indeed the flow identified here may contribute the observed colocation of the pinholes and tip facets. Regardless of these details, the flow up the tip facets provides an immediate opportunity for atoms from the pinholes to condense on these surfaces [before reaching the (110) surface facet] and in this way to extend the length of the fingers.

Before leaving the topic of surface morphology we com-

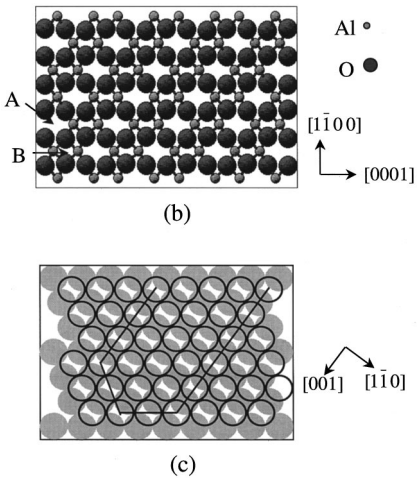

FIG. 13. (a) Structure of the sapphire $(11\bar{2}0)$ surface showing the rows of empty sites. These and the sapphire (0001) axis define the orientation of Nb shown in (b). The twin orientation reflected along [0001] is suppressed. A Nb surface finger is indicated in (b).

ment speculatively on the possible role of step-flow processes in forming the elaborate structures that are visible where the tip facets form the sidewalls of the pinholes in Fig. 5. These structures appear consistent with step flow up the sidewalls from the pinhole, together with step bunching that creates the cliffs which terminate the successive wide terraces in the detailed sidewall structures.

Our results show that the strain present in these Nb films is inhomogeneous, and depends on the growth temperature and film thickness. It must originate initially in the misfit between the Nb and the sapphire substrate, subsequently in strain relief of initially independent islands, is then complicated by their partial coalescence, and finally is relieved progressively by dislocation processes of the completed film. Partial accommodation of differential contraction between the niobium epilayer and the sapphire substrate as the film is cooled to room temperature completes this complex picture. At present there is no comprehensive explanation of the x-ray and electron microscope observations. The existence of strong strain fields and dislocations around the pinholes, as required by the above discussion of fingering, is nevertheless an experimental fact that remains valid regardless of the origins of the strain.

Epitaxy of Nb on Al_2O_3 is dominated by the alignment of a Nb [111] direction with sapphire [0001], and the occupation by Nb of empty surface sites on the Al sublattice. This geometry is shown in Fig. 13 with Nb stretched by 10.7% along [001] and by 8.3% along $[1\bar{1}0]$. Figure 8 shows that these huge strains are relieved by a factor 10 by the time the film reaches 500 A thick, even at 700 °C, and much more so at 1000 °C. It is natural in Fig. 8(b) that more strain at room temperature is retained in the 500-Å film than in the 1000-Å film, since the second 500 Å of the thicker films must continue the relaxation processes that started in the first 500 Å. The continuation of relaxation with thickness is documented in Fig. 8(b).

The narrow component of the x-ray rocking curve has been investigated earlier[13,14] and in other epitaxial systems like ErAs grown on GaAs.[23] It is believed to arise from spaced regions of perfect Nb that are maintained in accurate registry perpendicular to the growth plane by the highly coherent sapphire substrate. Each contributing region extends through much of the film thickness and this determines the observed Bragg peak widths in the direction normal to the surface. However, the lateral spacing between these coherent regions is believed to increase as the film grows thicker and more of the Nb is inhomogeneously strained. This accounts for the decreased proportion of narrow component in thicker films. Note that the width of the sharp peak is nevertheless determined by the lateral distance over which the coherent regions are maintained by the sapphire in accurate registry *parallel* to the growth direction. For off-normal Bragg peaks the sharp component is eliminated because random Nb displacements *perpendicular* to the growth direction, which are permitted by the sapphire, now have nonzero projections along the scattering vector.

We now discuss the three-dimensional structure associated with the broad component. The characteristics of the broadened peak, as determined in Sec. III, are (i) width normal to the growth plane limited by the equipment resolution and the film thickness (Fourier transform), combined with (ii) anisotropic in-plane width as documented in Sec. III C. These are consistent with (110) lattice planes that are buckled, with curvatures that are spread fairly randomly through the film area and thickness. Any deviation from randomness from one coherence volume to the next would necessarily broaden the longitudinal scans in a way that is not observed in the data. As noted in Sec. III, the results are consistent with the occurrence of (110) planes that buckle mostly perpendicular to an in-plane $\langle 111 \rangle$ direction that is itself substantially orthogonal to the tilt direction.

We attribute the buckled planes to an anisotropic distribution of dislocations that is present after the islands coalesce. The tilted lattice planes responsible for the wide rocking curves must originate in the displacement fields of dislocations with Burgers vectors having large components perpendicular to the growth plane. In Nb the preferred Burgers vectors are $\frac{1}{2}a\langle 111 \rangle$, with $\langle 111 \rangle$ line vectors and glide on $\{110\}$ planes, and those most responsible for the tilted (110) planes must have $\frac{1}{2}a\langle 111 \rangle$ or $\frac{1}{2}a\langle 11\bar{1} \rangle$ Burgers vectors and $\{\bar{1}1\bar{1}\}$ or $[1\,\bar{1}\,1]$ line vectors.[24,25] Presumably the observed offset of the broad and narrow peaks along the tilt direction has this same cause. Note that these dislocations have edge components in the growth plane and are therefore the most active in the relief of epitaxial strain. Now the substrate miscut modifies the distribution and motion of dislocations because the misfit component of the Burgers vector [i.e., its projection on (110)] depends on miscut, and so therefore does the stress on any given dislocation. The larger the misfit Burgers vector, the greater are the driving forces for dislocation nucleation and glide. Although most details remain obscure, it is nevertheless easy to see that the direction and size of miscut can play a significant role in determining the types of dislocation that are produced in any given epitaxial process, and hence the distribution of tilts present in the material. In the present case the dislocation systems identified here will not respond equally except in the case of miscut along a symmetry direction like [001], and in either case will, in general, create an anisotropic distribution of local tilts. We believe that this offers a possible explanation for the angular dependence of the broad rocking curves reported in

this paper, even though the dislocation processes in the inhomogeneous epilayer remain too complicated to follow in detail at the present time.

One final matter for comment here concerns the sidebands visible on the broadened rocking curve of Fig. 10. Following Gibaud *et al.*[14] we note that if miscut creates terraces of width T along the miscut direction, with steps of height a, the (small) angle of miscut is $\theta = a/T$ (for T large). Regularly spaced steps produce periodic in-plane structures with wave vectors that are multiples of $G_m = 2\pi/T$. As sidebands on a Bragg peak at the reciprocal-lattice vector $G_{110} = 2\pi/a$ these are located at (small) angular displacements from the Bragg peak that are multiples of the miscut angle $G_m/G_{110} = a/T$. Thus the observation of sidebands that are separated from the main peak by the angle of the miscut is consistent with an interpretation in which they are caused by steps of the vicinal surface. In width the sidebands mimic the broadened main Bragg peak, as is appropriate to this interpretation.

V. SUMMARY

We have identified a regime of temperature and thickness in which Nb (110) grows on miscut sapphire $(11\bar{2}0)$ with {110} faceted [001] fingers up to ~10 μm long. Using atomic force microscopy, transmission electron microscopy, and x-ray diffraction, the origins of the surface fluxes that create these features are traced to faceting and the strain fields that exist in the neighborhood of transient pinholes that occur where islands grow together in the early evolution of the films. These mesoscopic features have an added importance as surface templates when the films are employed as buffers during the heteroepitaxial growth of thin-film systems on sapphire substrates.

ACKNOWLEDGMENT

This research was supported in part by the Department of Energy, through the Materials Research Laboratory of the University of Illinois.

[1] S. M. Durbin, J. E. Cunningham, M. E. Mochel, and C. P. Flynn, J. Phys. F **11**, L223 (1981); **12**, L75 (1982).
[2] I. K. Schuller, Phys. Rev. Lett. **44**, 1597 (1980).
[3] J. E. Cunningham and C. P. Flynn, J. Phys. F **15**, L221 (1985).
[4] P. Grunberg, R. Schrieber, Y. Pang, M. B. Brodsky, and H. Sowers, Phys. Rev. Lett. **57**, 2442 (1986); P. Sonntag, M. Donner, N. Metoki, and H. Zabel, Phys. Rev. B **49**, 2869 (1994).
[5] J. Kwo, E. M. Gyorgy, D. B. McWhan, M. Hong, F. J. DiSalvo, C. Vetter, and J. E. Bower, Phys. Rev. Lett. **55**, 1402 (1985).
[6] K. A. Ritley and C. P. Flynn, Appl. Phys. Lett. **72**, 170 (1988).
[7] K. Theis-Brohl, K. A. Ritley, C. P. Flynn, K. Hamacher, H. Kaiser, and J. J. Rhyne, J. Appl. Phys. **79**, 4779 (1996).
[8] Reviewed by C. P. Flynn, MRS Bull. **16**, 90 (1991).
[9] X. Zhu, R. Feidenhans'l, H. Zabel, J. Als-Nielson, R. Du, C. P. Flynn, and F. Grey, Phys. Rev. B **37**, 7157 (1988).
[10] M. Huth and C. P. Flynn, J. Appl. Phys. **83**, 7261 (1998).
[11] D. B. McWhan, M. Gurvitch, J. M. Rowell, and L. R. Walker, J. Appl. Phys. **54**, 3886 (1983).
[12] F. J. Lamelas, H. He, and R. Clarke, Phys. Rev. B **38**, 6334 (1988).
[13] P. M. Reimer, H. Zabel, C. P. Flynn, and J. Dura, Phys. Rev. B **45**, 11 426 (1992).
[14] A. Gibaud, R. A. Cowley, D. F. McMorrow, R. C. C. Ward, and M. R. Wells, Phys. Rev. B **48**, 14 463 (1993).
[15] B. Wolfing, K. Theis-Brohl, C. Sutter, and H. Zabel, Thin Solid Films (to be published).
[16] J. Mayer, C. P. Flynn, and M. Ruhle, Ultramicroscopy **33**, 51 (1990); G. Gutekunst, J. Mayer, and M. Ruhle, Philos. Mag. A **75**, 1329 (1997).
[17] Y. Ikuhara, P. Pirouz, A. H. Heuer, S. Yadavalli, and C. P. Flynn, Philos. Mag. A **70**, 75 (1994); T. Wagner, M. Lorenz, and M. Ruhle, J. Mater. Res. **11**, 1255 (1996).
[18] G. L. Zhou, S. M. Bonham, and C. P. Flynn, J. Phys.: Condens. Matter **9**, L671 (1988).
[19] P. B. Hirsch, A. Howie, R. B. Nicholson, D. W. Pashley, and M. J. Whelan, *Electron Microscopy of Thin Crystals* (Butterworth, London, 1965).
[20] See, e.g., D. B. Williams and C. B. Carter, *Transmission Electron Microscopy* (Plenum, New York, 1996), Chap. 10.
[21] M. J. Stowell, in *Epitaxial Growth: Part II*, edited by J. W. Matthews (Academic, New York, 1975).
[22] See, e.g., E. G. Bauer, B. W. Dodson, D. E. Ehrlich, I. C. Feldman, C. P. Flynn, M. W. Geis, R. I. Matyi, P. S. Peercy, P. M. Petroff, J. M. Phillips, G. B. Stringfellow, and A. Zangwill, J. Mater. Res. **5**, 852 (1990).
[23] P. F. Miceli, in *Semiconductor Interfaces, Microstructures and Devices: Properties, and Applications*, edited by C. Feng (IOP, Bristol, 1993).
[24] J. P. Hirth and J. Lothe, *Theory of Dislocations*, 2nd ed. (Krieger, Malabar, 1992).
[25] J. W. Matthews and A. E. Blakeslee, J. Cryst. Growth **27**, 118 (1974); **32**, 265 (1976); J. W. Matthews, A. E. Blakeslee, and S. Mader, *ibid.* **33**, 253 (1976).